Shape transition of Nd and Sm isotopes and the neutrinoless double-β-decay nuclear matrix element of ^{150}Nd

Yusuke Tsunoda●

Center for Computational Sciences, University of Tsukuba, 1-1-1 Tennodai, Tsukuba 305-8577, Japan

Noritaka Shimizu●*

Center for Computational Sciences, University of Tsukuba, 1-1-1 Tennodai, Tsukuba 305-8577, Japan
and Center for Nuclear Study, The University of Tokyo, 7-3-1 Hongo, Tokyo 113-0033, Japan

Takaharu Otsuka●

Department of Physics, The University of Tokyo, 7-3-1 Hongo, Tokyo 113-0033, Japan;
RIKEN Nishina Center, 2-1 Hirosawa, Wako, Saitama 351-0198, Japan;
and Advanced Science Research Center, Japan Atomic Energy Agency, Tokai, Ibaraki 319-1195, Japan

Neutron-rich Nd and Sm isotopes are known to exhibit shape phase transition as a function of neutron number. Among them, ^{150}Nd and ^{150}Sm are important not only because they are transitional nuclei but also because they are the parent and daughter nuclei of double-β decay. We performed large-scale shell-model calculations of even-even Nd and Sm isotopes, including the spherical-deformed shape transition. The quasiparticle vacua shell model enables us to perform shell-model calculations with sufficiently large model space with the ^{110}Zr inert core. The shell-model result well reproduces the experimental excitation energies and quadrupole properties of the yrast and nonyrast states. The nuclear matrix element of neutrinoless double-β decay of ^{150}Nd is evaluated showing its modest enhancement by shape mixing.

Atomic nuclei show various shapes of their surfaces as the proton number (Z) and the neutron number (N) change, for example, from a sphere to a weakly distorted ellipsoid to a strongly distorted one. The Nd and Sm isotopes of $N \geqslant 82$ are one of the clear examples of this change, or evolution, from spherical shapes to ellipsoidal deformed shapes [1]. While this shape evolution is an interesting and important subject, systematic studies covering both spherical and deformed cases on equal footing must handle two different many-body structures, spherical and deformed, which correspond to significantly different types of mean-field solutions [1]. Besides this difficulty, the situations between these two limits, usually called transitional, must be described equally well, which likely requires more sophisticated multinucleon treatments.

The interacting boson model (IBM) [2] provides the eigensolution of its Hamiltonian within empirical approaches and was applied to the shape evolution of Sm isotopes [3], nicely describing it as a U(5)-SU(3) transition. Plenty of theoretical works have been devoted to understanding this evolution [4–8]. Besides this, the shell model is, in principle, an ideal approach, because it solves the multinucleon Schrödinger equation with a given effective nucleon-nucleon (NN) interaction, without referring to the specific features (e.g., shape) of the solutions to be obtained. On the other side, the practical application of the conventional shell-model calculations is limited by the number of valence nucleons and/or the number of valence single-particle orbits, which can result in the exploding dimension of the Hamiltonian matrix to be diagonalized. This limitation emerges for the study of the Nd-Sm shape evolution. Quite recently, however, a breakthrough was made by using the Monte Carlo shell model (MCSM) (see reviews [9–11]) as a different formulation of the shell-model calculation, and the description of the shape evolution in Sm isotopes was given in the light of realistic NN interactions [12].

In recent years, neutrinoless double-β decay has attracted keen and broad interests, as it is a crucial key to elucidating whether the neutrino is a Majorana particle or not [13]. The double-β decay from ^{150}Nd to ^{150}Sm may be used to extract the nuclear matrix element (NME) of the neutrinoless double-β ($0\nu\beta\beta$) decay, which is sensitive to the structure of involved nuclei [14]. This letter presents a new value of the NME of this decay.

Many experiments to search for neutrinoless double-β decay have been planned and undergone. Each of them has employed one of a dozen of the nuclides which can undergo double-β decay and has provided us with the lower limit of the half-life for $0\nu\beta\beta$ decay. To derive the information on neutrino mass from the half-life, the NME value for each nuclide has to be estimated theoretically. However, this estimation brings about large uncertainties of factor 2 [15]. Currently,

*shimizu@nucl.ph.tsukuba.ac.jp

the smallest upper limit of the effective neutrino mass reaches around 0.1 eV by the experiment with ^{136}Xe [16]. If we restrict ourselves to the case of ^{150}Nd, there have been quite a few efforts to evaluate its NME, such as the IBM [17], the quasiparticle random-phase approximation (QRPA) [18], and the generator coordinate method (GCM) [14,19–22]. Another GCM study employing a relativistic density functional revealed that the contribution of the octupole correlations cancels 7% of the NME [20]. The recent study of the projected shell model showed the importance of triaxial deformation [23]. Thus, various many-body correlations indeed need to be treated for the precise estimation of the NME.

The earlier MCSM calculation successfully describes the yrast states of Sm isotopes [12]. However, the precise evaluation of the NME of the $0\nu\beta\beta$ decay requires an improved efficiency towards more precise treatment of pairing correlations. In the present work, the quasiparticle vacua shell model (QVSM) [24] is adopted for this purpose, as its high efficiency towards high precision really pays for heavier computer resources needed. We made a test calculation of the present NME in Ref. [24] using the QVSM and found, in terms of moment of inertia, that the model space had to be enlarged. In the present study, we enlarge the model space by including the breaking of the ^{132}Sn core so that the experimental moment of inertia of the Nd and Sm isotopes can be reproduced well, and we evaluate the $0\nu\beta\beta$-decay NME of ^{150}Nd.

In the QVSM framework, a shell-model eigen wave function is described as a linear combination of the angular-momentum-, parity-, and number-projected quasiparticle vacua [1] as

$$|\Psi_{N_b}\rangle = \sum_{n=1}^{N_b} \sum_{K=-J}^{J} f_{nK}^{(N_b)} P_{MK}^{J\pi} P^Z P^N |\phi_n\rangle, \qquad (1)$$

where P^Z, P^N, and $P_{MK}^{J\pi}$ denote, respectively, the projectors of the proton number, the neutron number, and the angular momentum and parity combined. $|\phi_n\rangle = |\phi_n^{(\pi)}\rangle \otimes |\phi_n^{(\nu)}\rangle$ is a product of the quasiparticle vacua of protons and neutrons [1]. The coefficient $f_{nK}^{(N_b)}$ is an amplitude in the linear combination, and its value is determined by solving the generalized eigenvalue problem:

$$\sum_{n=1}^{N_b} \sum_{K=-J}^{J} \langle\phi_m|HP_{MK}^J P^Z P^N|\phi_n\rangle f_{nK}^{(N_b)}$$
$$= E^{(N_b)} \sum_{n=1}^{N_b} \sum_{K=-J}^{J} \langle\phi_m|P_{MK}^J P^Z P^N|\phi_n\rangle f_{nK}^{(N_b)}, \qquad (2)$$

with $E^{(N_b)}$ being the energy eigenvalue. The quasiparticle vacua $|\phi_n\rangle$ are determined so that $E^{(N_b)}$ is minimized. In the case of $N_b = 1$, it corresponds to the Hartree-Fock-Bogoliubov (HFB) calculation with the variation after the angular-momentum, parity, and number projection. In that sense, the QVSM is an extension of the variation after projection with the superposition. It is stressed that each QVSM basis vector can carry pairing correlations in it to good extents, but the pairing correlations are incorporated mainly through superpositions among different basis vectors in the MCSM (by Slater determinants). As the present NME has features

common with pairing correlations, the QVSM is expected to yield NME values that are more precise for a given number of basis vectors than the MCSM, meaning a faster convergence. It was shown in Ref. [24] that the $0\nu\beta\beta$-decay NME converged smoothly even with a small number of the QVSM basis vectors.

The model space and the interaction are taken from our previous MCSM study [12] with a minor modification. The model space consists of the sdg shell, $0h_{11/2}$, $1f_{7/2}$, and $2p_{3/2}$ orbits for protons, and the pfh shell, $0i_{13/2}$, $1g_{9/2}$, $2d_{5/2}$, and $3s_{1/2}$ orbits for neutrons, so that it contains $\Delta j = \Delta l = 2$ pairs in the respective upper shells. The Hamiltonian is constructed by combining the monopole-based universal (V_{MU}) interaction [25], whose proton-neutron interaction is multiplied by a factor of 0.94 to its isoscalar central part (as in Ref. [12]), and the G-matrix-based interaction for the proton-proton and neutron-neutron interactions [26]. The proton-pairing (neutron-pairing) matrix elements are multiplied by a factor of 0.9 (0.7) and some of the single-particle energies are slightly tuned from Ref. [12]. The pairing correlations are handled more efficiently by the QVSM compared to the MCSM with Slater determinants. For heavy nuclei, previous MCSM calculations may have led to stronger pairing interactions, because of a fit with a finite number of the basis vectors. Thus, the weaker pairing interactions suggested by the QVSM are natural consequences for heavy nuclei. The contamination of the center-of-mass excitation is removed by adding the Lawson term with $\beta_{CM}\hbar\omega/A = 1.0$ MeV, resulting in its quanta $O(10^{-3})$, which is sufficiently small.

In the present calculation for the $84 \leqslant N \leqslant 92$ nuclei, 24 QVSM basis states are optimized so as to lower the two lowest energy eigenvalues of 0^+, 2^+, and 4^+. The many-body subspace is then spanned by these 72 basis states and the eigenvalue problem in Eq. (2) is solved. For $N = 82$ and 94, 16 QVSM basis states are used to optimize the lowest energy eigenvalues of 0^+, 2^+, and 4^+, and totally 48 basis states are used to make up the QVSM wave function. The effective charges are taken as $(e_p, e_n) = (1.6, 0.6)e$ throughout the present work. Figure 1 shows the evolution of the excitation energies, the $E2$ transition probabilities, and the spectroscopic quadrupole moments of the Nd isotopes. At the $N = 82$ semimagic nucleus, the 2^+ and 4^+ excitation energies are rather large, and the seniority scheme is expected to work. With increasing neutron number, the excitation energies gradually decrease, and the ratio of the 4_1^+ and 2_1^+ energies indicates the transition from the spherical vibrator to the rotational band. The gradual increase of the $E2$ transition probabilities and quadrupole moments supports this interpretation. The theoretical excitation energies of the nonyrast states of ^{152}Nd ($N = 92$) are a few hundred keV lower than the experimental values, suggesting possible unmeasured levels. In the previous MCSM study [12], the gradual change of the excitation energies of 2^+ and 4^+ states was not perfectly reproduced because of the underestimation of the pairing correlation in the MCSM, and the nonyrast states were out of scope. The QVSM framework enables us to estimate the pairing correlation correctly and to give a unified description of these states.
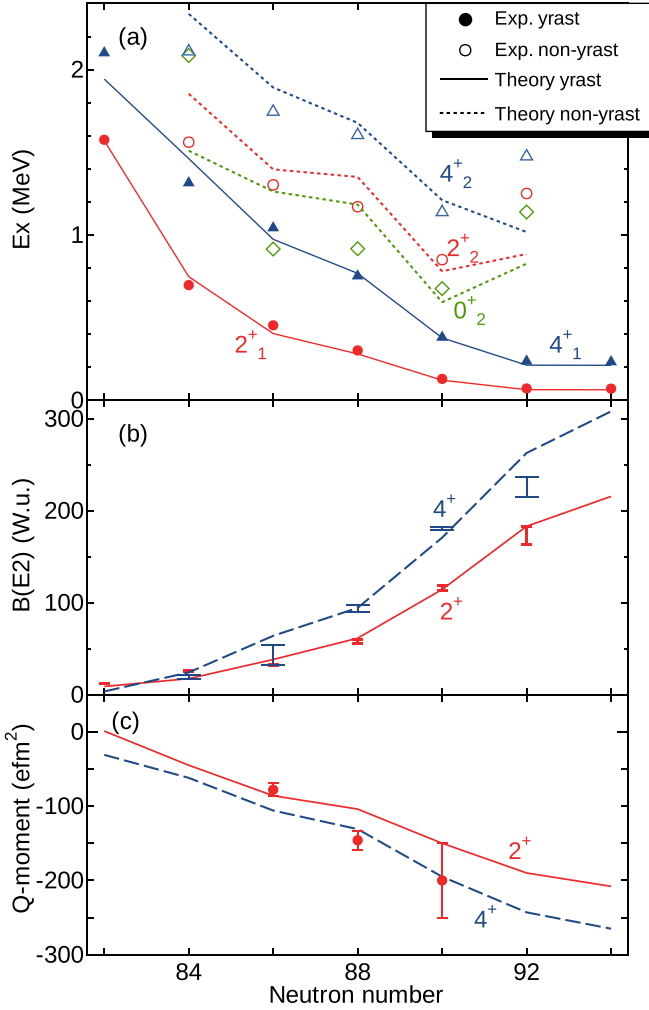
FIG. 1. (a) Excitation energies, (b) $B(E2; 2_1^+ \rightarrow 0_1^+)$ and $B(E2; 4_1^+ \rightarrow 2_1^+)$ values, and (c) spectroscopic quadrupole moments of the 2_1^+ and 4_1^+ states of Nd isotopes against the neutron number. (a) The red (lower) and blue (upper) solid lines denote the theoretical values of the 2_1^+ and 4_1^+ states, respectively. The red circles and blue triangles denote the experimental ones. The green, red, and blue dotted lines (open diamonds, circles, and triangles) denote the theoretical (experimental) values of the 0_2^+, 2_2^+, and values of the 0_2^+, 2_2^+, and 4_2^+ states, respectively. [(b), (c)] The solid red (dashed blue) lines are theoretical values of the 2_1^+ (4_1^+) states, while symbols denote the experimental values.

Figure 2 shows the excitation energies, $B(E2)$ values, and spectroscopic quadrupole moments of Sm isotopes. The 2_1^+ and 4_1^+ excitation energies gradually decrease, and the quadrupole collectivity grows as N increases. The Nd isotopes show similar trends. The most remarkable difference between Nd and Sm isotopes is seen at the nonyrast states: the excitation energies of the 0_2^+, 2_2^+, and 4_2^+ states drop down abruptly between $N = 86$ and 88 for the Sm isotopes, whereas such change occurs between $N = 88$ and 90 in the Nd isotopes. This tendency is nicely reproduced in the present results.

The QVSM wave function can be analyzed by using the T-plot figures, in which its component is visualized as scat-
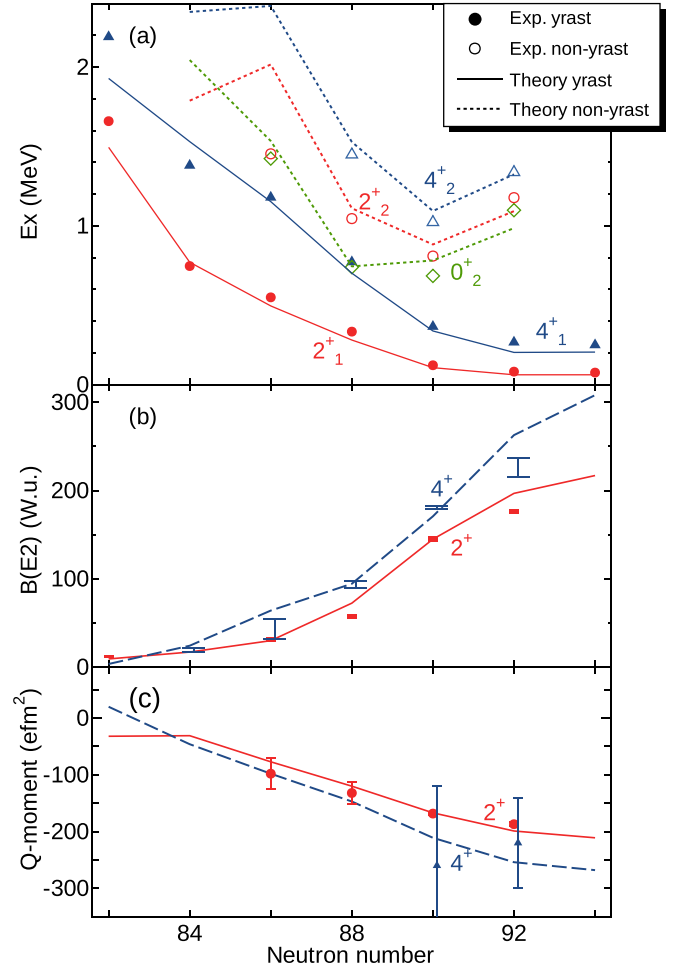
FIG. 2. (a) Excitation energies, (b) $B(E2)$ values, and (c) spectroscopic quadrupole moments of Sm isotopes. See the caption of Fig. 1.

tered circles on the energy surface in the same way as the MCSM [27,28]. Figure 3 shows the T plots of the 0_1^+ states of the Nd and Sm isotopes. The ground-state energy is drawn as contour lines given by the constrained number-projected HFB calculations with the constraints given by the usual intrinsic quadrupole moments, $Q_0 = \langle \phi | \hat{Q}_{20} P^Z P^N | \phi \rangle$ and $Q_2 = \langle \phi | \hat{Q}_{22} P^Z P^N | \phi \rangle$, where $\hat{Q}_{20}$ and $\hat{Q}_{22}$ are the quadrupole operators [1]. The shell-model Hamiltonian is taken for this calculation. The positions and areas of the circles on the energy surface represent, respectively, the deformation and the overlap probabilities between $|\phi_i\rangle$ and $|\Psi_{N_b}\rangle$ in Eq. (1). At $N = 84$ and 86, the minimum of the energy surfaces is close to $\langle Q_0 \rangle = \langle Q_2 \rangle = 0$ and their T-plot points are concentrated around the spherical shape. As N increases, the minimum of the energy surface and T-plot distributions gradually move toward prolate deformation. Among them, the T plots of ^{150}Nd and ^{150}Sm show a characteristic feature: the distribution is divided into two groups. We focus on their structures since these nuclides are the parent and daughter nuclei of the double-β decay.

Figure 4 shows the partial level scheme of the QVSM in comparison with the experimental ones. The nucleus
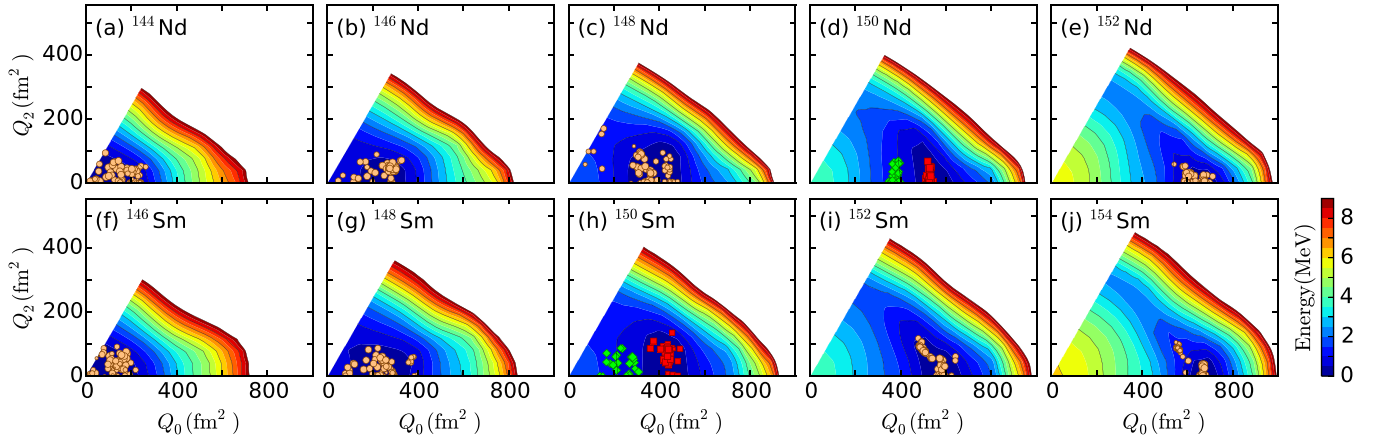
FIG. 3. T plots of the 0_1^+ states of $^{144-152}$Nd and $^{146-154}$Sm by the QVSM wave functions. On the figures of ^{150}Nd and ^{150}Sm, the green diamonds and red squares denote the "S" and "L" groups, respectively. See the main text for details.

^{150}Nd has been considered a candidate for the critical point symmetry X(5) [29,30]. This model assumes that the energy surface is flat in the direction of β on the prolate side, while the present work gives a shallow minimum by ≈ 4 MeV at the prolate deformation [see Fig. 3(d)]. Figure 4 includes the result of the X(5) model. These three results agree with each other reasonably well, up to $B(E2)$ values.

The NME of $0\nu\beta\beta$ decay is evaluated with the closure approximation as

$$M^{0\nu} = \langle 0_f^+ | \hat{O} | 0_i^+ \rangle = M_{GT}^{0\nu} - \frac{g_V^2}{g_A^2} M_F^{0\nu} + M_T^{0\nu}, \qquad (3)$$

where GT, F, and T denote, respectively, the contributions of the Gamow-Teller type, the Fermi type, and the tensor type [31]. Here, $|0_i^+\rangle$ and $|0_f^+\rangle$ are ground-state wave functions of ^{150}Nd and ^{150}Sm, respectively. The intermediate energy of this approximation is taken from the empirical formula $E_c = 1.12 A^{1/2}$ MeV [32] and $g_A/g_V = 1.27$ is adopted. The
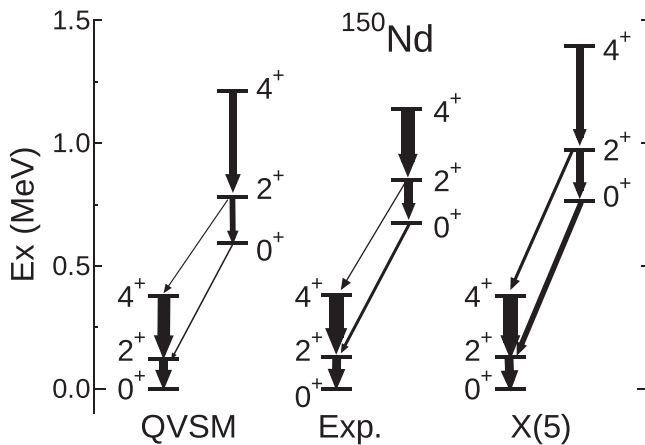
two-body current contribution to the transition operator is not included. Figure 5 displays the convergence of the $0\nu\beta\beta$-decay NME of ^{150}Nd as a function of the number of the QVSM basis vectors. It shows rather good convergence at $N_b = 72$. The present result for $N_b = 1$ is similar to but beyond the HFB calculation, because the variation after the angular-momentum, parity, and number projections is performed. The contribution of the effect of configuration mixing in the QVSM framework increases the NME by 20% in comparison with the value of $N_b = 1$. The QVSM basis vectors are obtained so that the two low-lying energies are minimized. Even if three low-lying energies are optimized, the resultant NME shows a difference of less than 5%. The NME calculated without short-range correlation becomes 4.00 as shown in Table I. In addition, we applied three types of short-range correlations (SRCs): Miller-Spencer [33], CD-Bonn, and Argonne [34]. The Miller-Spencer short-range correlation quenches the NME by $\approx 20\%$, and the CD-Bonn and Argonne correlations give 10% uncertainty. The tensor contributions are negligibly small like other theoretical studies.

In other theoretical methods, e.g., the quasiparticle random-phase approximation gives the $0\nu\beta\beta$-decay matrix element as 2.71 [35]. The interacting boson model provides 2.32 [17], which is close to the value of the QRPA. The NME
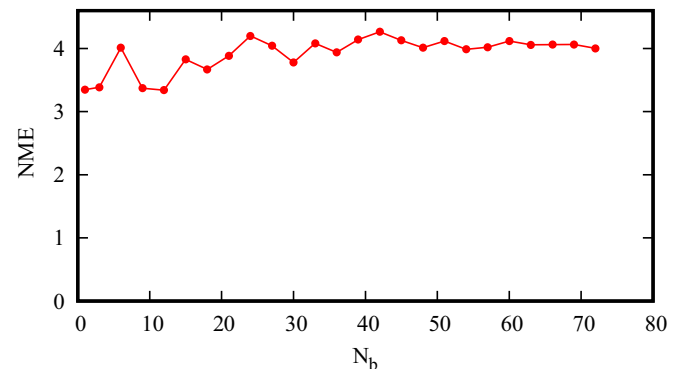

FIG. 4. Partial level schemes of ^{150}Nd obtained by the QVSM, the experiment, and the X(5) critical point symmetry [29,30]. The arrow widths are proportional to the $B(E2)$ values. Only those >10 W.u. are displayed. The X(5) results are scaled so that it reproduces the experimental values of $Ex(2_1^+)$ and $B(E2; 2_1^+ \to 0_1^+)$.

FIG. 5. $0\nu\beta\beta$-decay NME of ^{150}Nd without short-range correlation, $M^{0\nu}$, against the number of QVSM basis vectors.

TABLE I. Nuclear matrix elements of neutrinoless double-β decay with various short-range correlations.

SRC	$M_{GT}^{0\nu}$	$M_F^{0\nu}$	$M_T^{0\nu}$	$M^{0\nu}$
None	3.32	−1.11	−0.01	4.00
Miller-Spencer	2.65	−0.91	−0.01	3.21
CD-Bonn	3.40	−1.16	−0.01	4.11
Argonne	3.21	−1.10	−0.01	3.88

values given by the latest GCM based on the relativistic energy density functional are 5.6 [36] and 5.2 [20]. On the other hand, the NME by the GCM with the nonrelativistic Gogny functional is a rather small value, 1.71 [21]. It was indicated that the large difference in the quadrupole deformations of the initial and final states would suppress the NME [18,19,21]. Thus, the predictions of the NME vary from 1.7 to 5.6 and our NME value is around the middle of them.

Since the decay life of $2\nu\beta\beta$ decay of ^{150}Nd to the 0_2^+ state of ^{150}Sm has been experimentally measured [37], the $0\nu\beta\beta$ NME to the 0_2^+ state might be possible and worth mentioning. The $0\nu\beta\beta$-decay NME from the ground state of ^{150}Nd to the 0_2^+ state of ^{150}Sm is 1.1, which is smaller than that of the ground state. This situation is similar to the prediction of the relativistic energy density functional [NME = 5.2 (0_1^+) and 0.72 (0_2^+)] [20] and that of the interacting boson model [NME = 2.321 (0_1^+) and 0.395 (0_2^+)] [17]. For comparison, the experimental $2\nu\beta\beta$-decay NME is obtained as 0.055(3) for the ground state and 0.044(5) for the excited state [38]. To evaluate the $2\nu\beta\beta$-decay NME in the shell-model framework, we have to compute the intermediate states of ^{150}Pm since the closure approximation is not justified in this case. This is not feasible and is left for future work. Figure 6 shows the decomposition of the angular momentum J and the parity π of the NME of ^{150}Nd. The decomposition of J^π intermediate states is defined in the same way as in Refs. [39,40] as

$$M^{0\nu} = \sum_{J,\pi} \langle 0_f^+ | \sum_{i \leqslant j, k \leqslant l} M_{i,j,k,l}^{J,\pi} \left[(c_i^\dagger \otimes c_j^\dagger)^{(J,\pi)} \right.$$
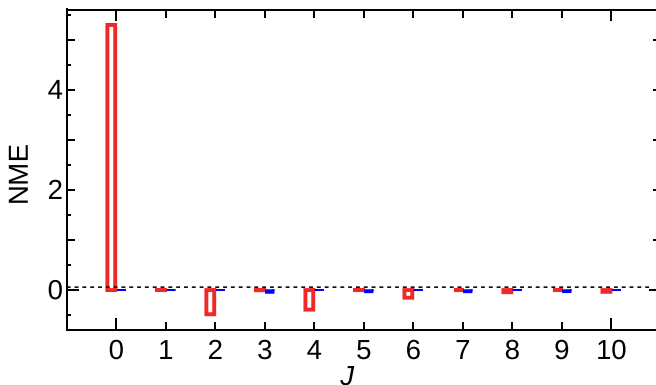$$\left. \times (c_k \otimes c_l)^{(J,\pi)} \right]^{(0)} | 0_i^+ \rangle. \quad (4)$$

FIG. 6. J^π decomposition of the $0\nu\beta\beta$-decay NME of ^{150}Nd. The open red (solid blue) bars denote positive-parity (negative-parity) components.

The contribution of the 0^+ pair plays a dominant role, while the 2^+ and 4^+ pairs have a certain negative contribution. In previous shell-model studies of the $0\nu\beta\beta$ decays of ^{48}Ca [39], ^{82}Se, and ^{130}Te [40], the contribution of the 2^+ pair is rather large (around −2) and cancels most of the contribution of the 0^+ pair. In the present case, the contribution of the 2^+ pair is rather small and its cancellation is not strong. The contribution of the intermediate negative-parity states is negligible.

We here mention the effect of the enlargement of the model space to the $0\nu\beta\beta$-decay NME. In Ref. [39], we demonstrated that the shell-model NME value of ^{48}Ca increases by about 30% by adding the sd shell to the conventional pf-shell model space. This is because the ^{48}Ca nucleus has a spherical shape and the pair excitation from the sd shell to the pf shell enhances the pairing correlation and, consequently, the NME also increases. On the other hand, in the ^{150}Nd case, the shell-model study assuming the ^{132}Sn core underestimates the quadrupole deformation, which causes the underestimation of the NME [24]. The present work employs sufficiently large model space so that the moment of inertia is correctly reproduced and thus the 30% reduction of the NME value is found.

Now we discuss the nuclear structures of ^{150}Nd and ^{150}Sm, utilizing more details of the T plots. The T plots in Fig. 3 show that the points are concentrated in two regions: the two groups of different deformations form the ground-state wave functions, where one group is for weaker deformation (green diamonds) and the other group is for stronger deformation (red squares). The group composed only of smaller (larger) ones is referred to by the index "S" ("L") hereafter. The ground-state wave functions are their linear combinations:

$$|0_1^+;{}^{150}\text{Nd}\rangle = 0.50|\text{S};{}^{150}\text{Nd}\rangle + 0.86|\text{L};{}^{150}\text{Nd}\rangle,$$
$$|0_1^+;{}^{150}\text{Sm}\rangle = 0.65|\text{S};{}^{150}\text{Sm}\rangle + 0.76|\text{L};{}^{150}\text{Sm}\rangle. \quad (5)$$

These two components with different deformations are almost degenerate in energy and are strongly mixed. The second 0^+ states are also described approximately as their linear combinations, which are orthogonal to the ground states, and show excitation energies lower than those of the neighboring isotopes. The NME $\langle \text{S};{}^{150}\text{Sm}|\hat{O}|\text{S};{}^{150}\text{Nd}\rangle$ turns out to be 3.87 without the SRC, which is largest among NMEs of other combinations. $\langle \text{L};{}^{150}\text{Sm}|\hat{O}|\text{L};{}^{150}\text{Nd}\rangle$, $\langle \text{L};{}^{150}\text{Sm}|\hat{O}|\text{S};{}^{150}\text{Nd}\rangle$, and $\langle \text{S};{}^{150}\text{Sm}|\hat{O}|\text{L};{}^{150}\text{Nd}\rangle$ are 2.81, 2.70, and −0.28, respectively. $\langle \text{S};{}^{150}\text{Sm}|\hat{O}|\text{L};{}^{150}\text{Nd}\rangle$ is small because the deformation of the bra and ket states is significantly different. One sees that the mixing amplitudes in Eq. (5) modestly enhance the NME to 4.00, and the present calculation appears to treat this feature appropriately.

In summary, we present a shell-model description of the spherical-to-deformed shape evolution of Nd and Sm isotopes including the nonyrast states in a unified way. The ground states of ^{150}Nd and ^{150}Sm are transitional in this shape-evolution scenario. They are characterized by two components of different prolate shapes and are mixed. This situation may be regarded to be a "double-prolate-shape coexistence with mixing." The $0\nu\beta\beta$-decay NME of ^{150}Nd is affected by this mixing and is evaluated as 4.1 with the CD-Bonn short-range

correlations. A more sophisticated $0\nu\beta\beta$-decay NME operator is expected to be derived for future studies, for instance, an additional short-range matrix element like that proposed in Refs. [41,42].

[1] P. Ring and P. Schuck, *The Nuclear Many-Body Problem* (Springer, Berlin, 2004).

[2] A. Arima and F. Iachello, The Interacting Boson Model*, Cambridge Monographs on Mathematical Physics* (Cambridge University, Cambridge, England, 1987).

[3] O. Scholten, F. Iachello, and A. Arima, Ann. Phys. **115**, 325 (1978).

[4] P. Cejnar, J. Jolie, and R. F. Casten, Rev. Mod. Phys. **82**, 2155 (2010).

[5] K. Nomura, N. Shimizu, and T. Otsuka, Phys. Rev. Lett. **101**, 142501 (2008).

[6] L. M. Robledo, R. R. Rodríguez-Guzmán, and P. Sarriguren, Phys. Rev. C **78**, 034314 (2008).

[7] Z. P. Li, T. Nikšić, D. Vretenar, J. Meng, G. A. Lalazissis, and P. Ring, Phys. Rev. C **79**, 054301 (2009).

[8] J. P. Delaroche, M. Girod, J. Libert, H. Goutte, S. Hilaire, S. Péru, N. Pillet, and G. F. Bertsch, Phys. Rev. C **81**, 014303 (2010).

[9] T. Otsuka, M. Honma, T. Mizusaki, N. Shimizu, and Y. Utsuno, Prog. Part. Nucl. Phys. **47**, 319 (2001).

[10] N. Shimizu, T. Abe, Y. Tsunoda, Y. Utsuno, T. Yoshida, T. Mizusaki, M. Honma, and T. Otsuka, Prog. Theor. Exp. Phys. **2012**, 01A205 (2012).

[11] N. Shimizu, T. Abe, M. Honma, T. Otsuka, T. Togashi, Y. Tsunoda, Y. Utsuno, and T. Yoshida, Phys. Scr. **92**, 063001 (2017).

[12] T. Otsuka, Y. Tsunoda, T. Abe, N. Shimizu, and P. Van Duppen, Phys. Rev. Lett. **123**, 222502 (2019).

[13] M. Dolinski, A. Poon, and W. Rodejohann, Annu. Rev. Nucl. Part. Sci. **69**, 219 (2019).

[14] N. L. Vaquero, T. R. Rodríguez, and J. L. Egido, Phys. Rev. Lett. **111**, 142501 (2013).

[15] J. Engel and J. Menéndez, Rep. Prog. Phys. **80**, 046301 (2017).

[16] A. Gando, Y. Gando, T. Hachiya, A. Hayashi, S. Hayashida, H. Ikeda, K. Inoue, K. Ishidoshiro, Y. Karino, M. Koga, S. Matsuda, T. Mitsui, K. Nakamura, S. Obara, T. Oura, H. Ozaki, I. Shimizu, Y. Shirahata, J. Shirai, A. Suzuki *et al.*, Phys. Rev. Lett. **117**, 082503 (2016).

[17] J. Barea and F. Iachello, Phys. Rev. C **79**, 044301 (2009).

[18] D.-L. Fang, A. Faessler, V. Rodin, and F. Šimkovic, Phys. Rev. C **83**, 034320 (2011).

[19] L. S. Song, J. M. Yao, P. Ring, and J. Meng, Phys. Rev. C **90**, 054309 (2014).

[20] J. M. Yao and J. Engel, Phys. Rev. C **94**, 014306 (2016).

[21] T. R. Rodríguez and G. Martínez-Pinedo, Phys. Rev. Lett. **105**, 252503 (2010).

[22] J. Yao, J. Meng, Y. Niu, and P. Ring, Prog. Part. Nucl. Phys. **126**, 103965 (2022).

[23] Y. K. Wang, P. W. Zhao, and J. Meng, Phys. Rev. C **104**, 014320 (2021).

[24] N. Shimizu, Y. Tsunoda, Y. Utsuno, and T. Otsuka, Phys. Rev. C **103**, 014312 (2021).

[25] T. Otsuka, T. Suzuki, M. Honma, Y. Utsuno, N. Tsunoda, K. Tsukiyama, and M. Hjorth-Jensen, Phys. Rev. Lett. **104**, 012501 (2010).

[26] B. A. Brown, Phys. Rev. Lett. **85**, 5300 (2000).

[27] Y. Tsunoda, T. Otsuka, N. Shimizu, M. Honma, and Y. Utsuno, Phys. Rev. C **89**, 031301(R) (2014).

[28] T. Otsuka and Y. Tsunoda, J. Phys. G: Nucl. Part. Phys. **43**, 024009 (2016).

[29] F. Iachello, Phys. Rev. Lett. **87**, 052502 (2001).

[30] R. Krücken, B. Albanna, C. Bialik, R. F. Casten, J. R. Cooper, A. Dewald, N. V. Zamfir, C. J. Barton, C. W. Beausang, M. A. Caprio, A. A. Hecht, T. Klug, J. R. Novak, N. Pietralla, and P. von Brentano, Phys. Rev. Lett. **88**, 232501 (2002).

[31] R. A. Sen'kov and M. Horoi, Phys. Rev. C **88**, 064312 (2013).

[32] W.C. Haxton and G. Stephenson, Jr., Prog. Part. Nucl. Phys. **12**, 409 (1984).

[33] G. A. Miller and J. E. Spencer, Ann. Phys. **100**, 562 (1976).

[34] F. Šimkovic, A. Faessler, H. Müther, V. Rodin, and M. Stauf, Phys. Rev. C **79**, 055501 (2009).

[35] M. T. Mustonen and J. Engel, Phys. Rev. C **87**, 064302 (2013).

[36] J. M. Yao, L. S. Song, K. Hagino, P. Ring, and J. Meng, Phys. Rev. C **91**, 024316 (2015).

[37] O. Polischuk, A. Barabash, P. Belli, R. Bernabei, R. Boiko, F. Cappella, V. Caracciolo, R. Cerulli, F. Danevich, A. Di Marco *et al.*, Phys. Scr. **96**, 085302 (2021).

[38] A. Barabash, Universe **6**, 159 (2020).

[39] Y. Iwata, N. Shimizu, T. Otsuka, Y. Utsuno, J. Menéndez, M. Honma, and T. Abe, Phys. Rev. Lett. **116**, 112502 (2016).

[40] A. Giuliani and A. Poves, Adv. High Energy Phys. **2012**, 857016 (2012).

[41] V. Cirigliano, W. Dekens, J. de Vries, M. L. Graesser, E. Mereghetti, S. Pastore, and U. van Kolck, Phys. Rev. Lett. **120**, 202001 (2018).

[42] L. Jokiniemi, P. Soriano, and J. Menéndez, Phys. Lett. B **823**, 136720 (2021).